Solid State Phenomena
ISSN: 1662-9779, Vol. 388, pp 81-89
doi:10.4028/p-LRdKA5

Submitted: 2026-01-15
Revised: 2026-02-11
Accepted: 2026-02-18
Online: 2026-04-15

Influence of Hydrogen Content on the Ductile Rupture of Advanced High-Strength Steels

GERMAIN Lisa[1,a*], VUCKO Flavien[2,b], PELTIER Fabienne[2,c], and THUILLIER Sandrine[1,d]

[1]Univ. Bretagne Sud, UMR CNRS 6027, IRDL, F-56100 Lorient, France

[2]French Corrosion Institute, Brest, France

[a]lisa.germain@univ-ubs.fr, [b]flavien.vucko@institut-corrosion.fr,
[c]fabienne.peltier@institut-corrosion.fr, [d]sandrine.thuillier@univ-ubs.fr

Keywords: Advanced High-Strength Steel, Ductility, Diffusible Hydrogen Content, Mechanical State

Abstract. Advanced high-strength steels exhibit sensitivity to diffusible hydrogen content, mainly observed during tensile testing. Although the initial yield stress and ultimate tensile strength are not significantly affected, ductility decreases with increasing hydrogen content. This sensitivity to diffusible hydrogen depends on strain rate and stress concentrations. This study examines the influence of diffusible hydrogen content on the ductile fracture of DP780GI steel, in the form of 1 mm thick sheets. Samples were prepared with specific geometries, with notches and holes, to study different mechanical states, and fracture tests were performed to evaluate ductility as a function of hydrogen content and stress triaxiality. The local strain rate was around $1 \times 10^{-4}\,\mathrm{s}^{-1}$, which is lower than the value used in industrial applications, to enhance the hydrogen sensitivity. A hydrogen charging process was used, including zinc coating removal, electrochemical loading, and electrolytic deposition of a zinc layer to prevent hydrogen desorption. The hydrogen content was measured by thermal desorption analysis after the mechanical testing. It is observed that the maximum local elongation decreases with increasing hydrogen content, with a noticeable effect above 0.25 ppm. Cracks form in areas of maximum effective deformation, and their location varies depending on the geometry of the sample and the hydrogen content. The evolution of the maximum effective strain before fracture shows a significant decrease in ductility with increasing hydrogen content, regardless of the mechanical state.

Introduction

The mechanical behavior of advanced high strength steels, in particular dual phase steels [1], is sensitive to the diffusible hydrogen content, and this influence has been mainly investigated in tension [2]. The general trend is that the initial yield stress and ultimate tensile stress are not significantly affected whereas the ductility decreases [3]. Smooth and notched specimen were considered for tensile tests, for several strain rates in the quasi-static domain and up to $900\,\mathrm{s}^{-1}$ [4], usually highlighting a critical hydrogen content above which the mechanical properties are significantly decreased. Moreover, the sensitivity to hydrogen content depends on the strain rate, increasing when the strain rate decreases, and on stress concentrations [5]. Two main mechanisms are proposed in literature as the origin of this phenomenon, which are hydrogen-enhanced localised plasticity and hydrogen-enhanced decohesion, cf. a review paper for steels and iron [6].

This sensitivity of the formability limits to diffusible hydrogen, which also leads to delayed fracture, e.g., [7], is a well-known feature of advanced high strength steels mainly investigated in tension. However, it must be characterised under several mechanical states, to be taken into account in virtual forming, which is the aim of the collaborative H2FORM3G project [8], for an application in the automotive industry. Although three advanced high strength steels are considered in H2FORM3G project, only results for a dual phase DP780 are presented as a first step.

The aim of this study is to investigate the influence of hydrogen content on the flow stress and the ductility for several mechanical states, described by the triaxiality ratio and Lode parameter, using dedicated rupture tests, for a dual phase steel. The microstructure of dual phase steels is mainly

made of martensite islands within a ferritic matrix, with volume fraction of martensite ranging from $18\,\%$ to $25\,\%$ depending on the composition [9]. Moreover, retained austenite may also expected as a consequence of the thermal treatment [10]. The experimental procedure, for mechanical testing and hydrogen charging, is first detailed and then results are presented, to highlight the sensitivity of the ductility to hydrogen content and mechanical state.

Materials and Experimental Procedure

Material.

A dual phase steel DP780GI (CR440Y780T-DP) is provided as sheets of thickness $t_0 = 1\,\text{mm}$, galvanized with a pure zinc layer. The mechanical properties were measured using tensile tests performed in the rolling direction, with 3 tests to check the repeatability, at a strain rate around $1 \times 10^{-3}\,\text{s}^{-1}$. Dog-bone specimen with a width of $12.5\,\text{mm}$ and a gauged length of $75\,\text{mm}$ were machined, following NF EN ISO 6892-1 standard. Mechanical properties are given in Table 1 while the chemical composition is available online[3].The maximum homogeneous strain in tension is close to 0.13, cf. the value of the plastic extension at maximum load A_g in Table 1, though locally, in an area of length $2\,\text{mm}$, a much higher value, around 0.4, is reached in the necking area just before rupture, cf. Fig. 1.

Table 1: Mechanical properties for DP780GI (CR440Y780T-DP). r_0 and r_{90} stand for the plastic anisotropy coefficients in the rolling and transverse directions, R_m is the ultimate tensile strength and R_{p02} the practical yield stress.

R_{p02} [MPa]	R_m [MPa]	r_0	r_{90}	A_g (%)
487.7 ± 4.0	783.3 ± 0.9	0.73 ± 0.01	0.84 ± 0.01	13.7 ± 0.1

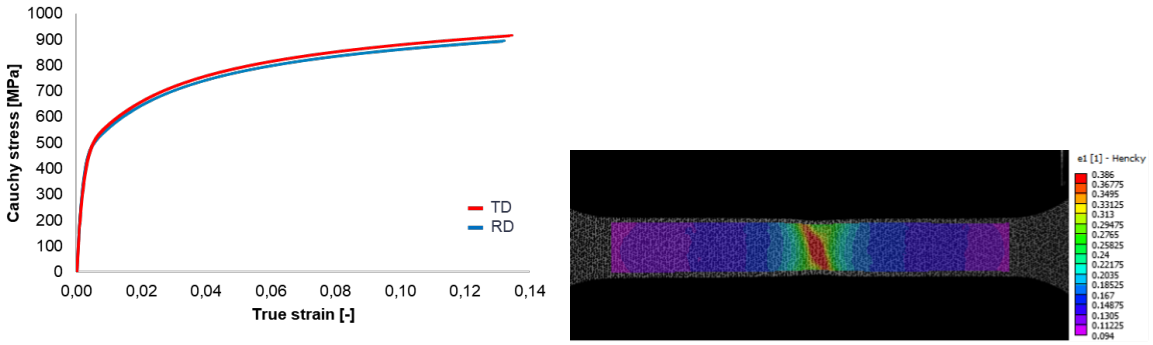

(a) (b)

Fig. 1: (a) Cauchy stress versus the logarithmic strain in uniaxial tension and (b) major strain field recorded by Digital Image Correlation just before rupture for DP780. The maximum strain value is around 0.4, which highlights the good formability of the material.

Mechanical testing.

Specimen are cut by electrical discharge machining for geometries with discontinuities (notches, holes) for the rupture tests. Indeed, the edge quality is of utmost importance for the rupture, especially with hydrogen embrittlement, as cracks are often observed starting from the surface [11].

For all the specimens, a random pattern of black dots is printed with a UV printer on the specimen surface, over a uniform sprayed white layer, to perform digital image correlation, using VIC-3D. A subset size of $21\,\text{px}$ and a step size of $5\,\text{px}$ for the notched specimen and respectively $23\,\text{px}$ and $4\,\text{px}$ for the specimen with a hole and $15\,\text{px}$ and $3\,\text{px}$ for the shear-type geometry were used. These values

[3] https://automotive.arcelormittal.com/products/flat/first_gen_AHSS/DP

were chosen from a performance analysis based on the evolution of the maximum strain evolution with the noise level. The strain window is 5. The acquisition frequency is 1 Hz.

The tests are performed on an electromechanical tensile machine of maximum capacity 50 kN (INSTRON 5969), using hydraulic grips to obtain a homogeneous clamping over the specimen width. Moreover, special care was taken to set the specimen in the grips so that the displacement was applied parallel to the direction corresponding to the specimen length.Two digital cameras are mounted on a rigid frame on the tensile machine, to capture the area of interest. Tests were carried out by controlling the displacement of the crosshead so that the strain rate in the most deformed area is nearly constant and approximately equal to $3 \times 10^{-4}\,\mathrm{s}^{-1}$. It should be emphasized that this value, lower than the value used for the tensile test and in industrial applications, was chosen to enhance the hydrogen sensitivity of the material [1]. Specimens with circular notches (N-R5 and N-R15), with a central hole (H-R4) and with complex cuts, leading mainly to a simple shear state (SH), are used to generate different mechanical states [12].The geometries are shown in Fig. 2. The load divided by the minimum initial area is plotted versus the elongation of a local extensometer ΔL defined from the digital image correlation information. The gauge length L_0 of this extensometer is defined so that it covers the area of strain localisation, with a value around 15 mm for all the rupture tests.

Finally, specific tests were carried out using a high-speed camera with a frequency of 8000 and up to 10000 frames per second, to investigate the spatial location of the cracks and wether it is dependent on the hydrogen content.

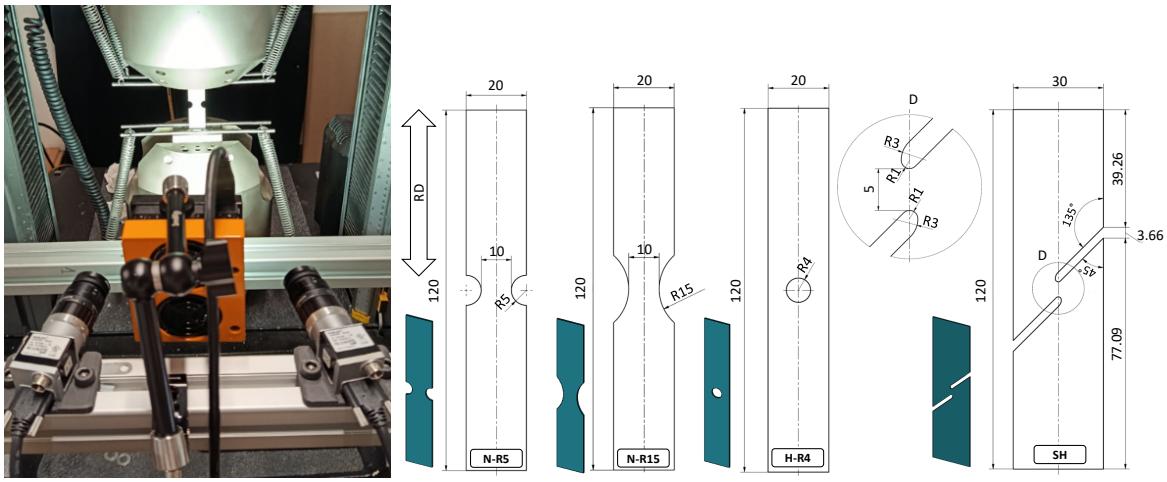

(a) (b)

Fig. 2: Rupture tests: (a) experimental setup for and (b) sample geometry.

Hydrogen charging.

A 3 step procedure was defined to control the content of hydrogen introduced in the specimen: removal of the zinc coating, as the materials are galvanized steels with a zinc layer thickness around 8 µm, electrochemical hydrogen charging and electrodeposition of a zinc layer to prevent hydrogen desorption at room temperature. First, a sample was etched from 1 to 5 min in a solution of HCl (1:3) and HMTA ($6\,\mathrm{g\,L}^{-1}$) in an ultrasonic bath. After etching, the sample was rinsed in distilled water, immersed in $0.1\,\mathrm{mol\,L}^{-1}$ NaOH solution for approximately 1 min and then immersed in ethanol and finally dried. Hydrogen content is expressed as a mass fraction, in ppm.

Cathodic charging was performed in a solution of 3% NaCl for a hydrogen content of 0.3 ppm and ammonium thiocyanate NH_4SCN $1\,\mathrm{g\,L}^{-1}$ is added to reach 0.5 ppm, under a voltage of -1300 mV with reference to the saturated calomel electrode (SCE) during 2 h. The current intensity depends on the sample size, i.e., $1\,\mathrm{mA\,cm}^{-2}$. For the lowest hydrogen content, i.e., 0.1 ppm, the zinc layer is removed and electroplating is redone, without additional steps in-between.

Finally, electroplating was performed at a current density of 25 mA cm^{-2} during 12 min in a neutral solution of electrolytic zinc, to obtain a dense zinc layer of a similar initial thickness. The zinc coating acts as a barrier that prevents the desorption of diffusible hydrogen at room temperature from the coated samples.

After mechanical testing, the hydrogen content was measured by thermal desorption analysis (TDA) [13] on the deformed specimen, using a katharometer G8 Galileo from Bruker equipped with a mass spectrometer. Small rectangular samples were cut in undeformed areas, under the grips, and were pickled in HCl/HMTA prior to TDA. For the measurement of diffusible hydrogen content, the quantification was carried out by heating samples up to $800\,°$C with a rate of $1\,°$C s^{-1}. To extract the diffusible hydrogen content, only the first desorption peak (below $500\,°$C) was considered. The calibration of the device was done with 5%H_2 in N_2 gas. The accuracy of the measure is $\pm\ 0.02$ ppm.

Results and Discussion

Influence of hydrogen content is first analysed through the stress levels. Moreover, an effective strain, defined by Eq. 1, is calculated for the rupture tests and the maximum value (except for SH geometry, as explained further) is output as an average over a circular area of diameter 0.5 mm.

$$\epsilon_{eq} = \frac{2}{\sqrt{3}}\sqrt{\epsilon_1^2 + \epsilon_2^2 + \epsilon_1\epsilon_2} \tag{1}$$

For each test, just before rupture, the maximum effective strain is output. It should be emphasised that it does not represent a rupture strain, as it is measured on the surface and the maximum strain is usually reached in the thickness. Indeed, the fracture strain is usually predicted numerically within a hybrid experimental-numerical approach, e.g., [12]. However, this maximum surface strain is used in this study as an indicator of the ductility of the material.

The load, divided by the initial minimum area (referred to as normalised load), evolution with the elongation of the local extensometer is presented in Fig. 3. The normalised load is sensitive to the mechanical state, that can be described using the triaxiality ratio η and Lode's parameter L, defined as $\eta = \dfrac{\text{trace}\,(\sigma)}{3\sigma_{eq}}$ and $L = \dfrac{2\sigma_2 - \sigma_1 - \sigma_3}{\sigma_1 - \sigma_3}$ [12]. This influence is consistent with previous results, but the concentration of diffusible hydrogen was not given [14]. Finite element simulations were performed, for each test, and the Cauchy stress components were output in the local area where rupture occurred. Averaged values of the triaxiality ratio and Lode parameter were calculated, but for a different material, i.e, an aluminium alloy, and are given in Table 2. It should be emphasized that these values may be material dependent, especially for N-R5 and N-R15; however, the general trend that the triaxiality ratio is higher for N-R5 and N-R15 than for H-R4, this last one being also higher than the one for SH, does not seem to depend on the material. Finite element calculations will be performed to confirm this point.

Table 2: Averaged values of η and L for rupture tests, from [12].

	N-R5	N-R15	H-R4	SH
η	0.58	0.50	0.35	0.06
L	-0.15	-0.46	-0.92	-0.14

The normalised load level is higher for higher values of η, for the base and hydrogen-charged materials. It can also be seen that the maximum local elongation decreases when the hydrogen content increases, with a sensitive effect above 0.25 ppm. To highlight this tendency, a global indicator defined

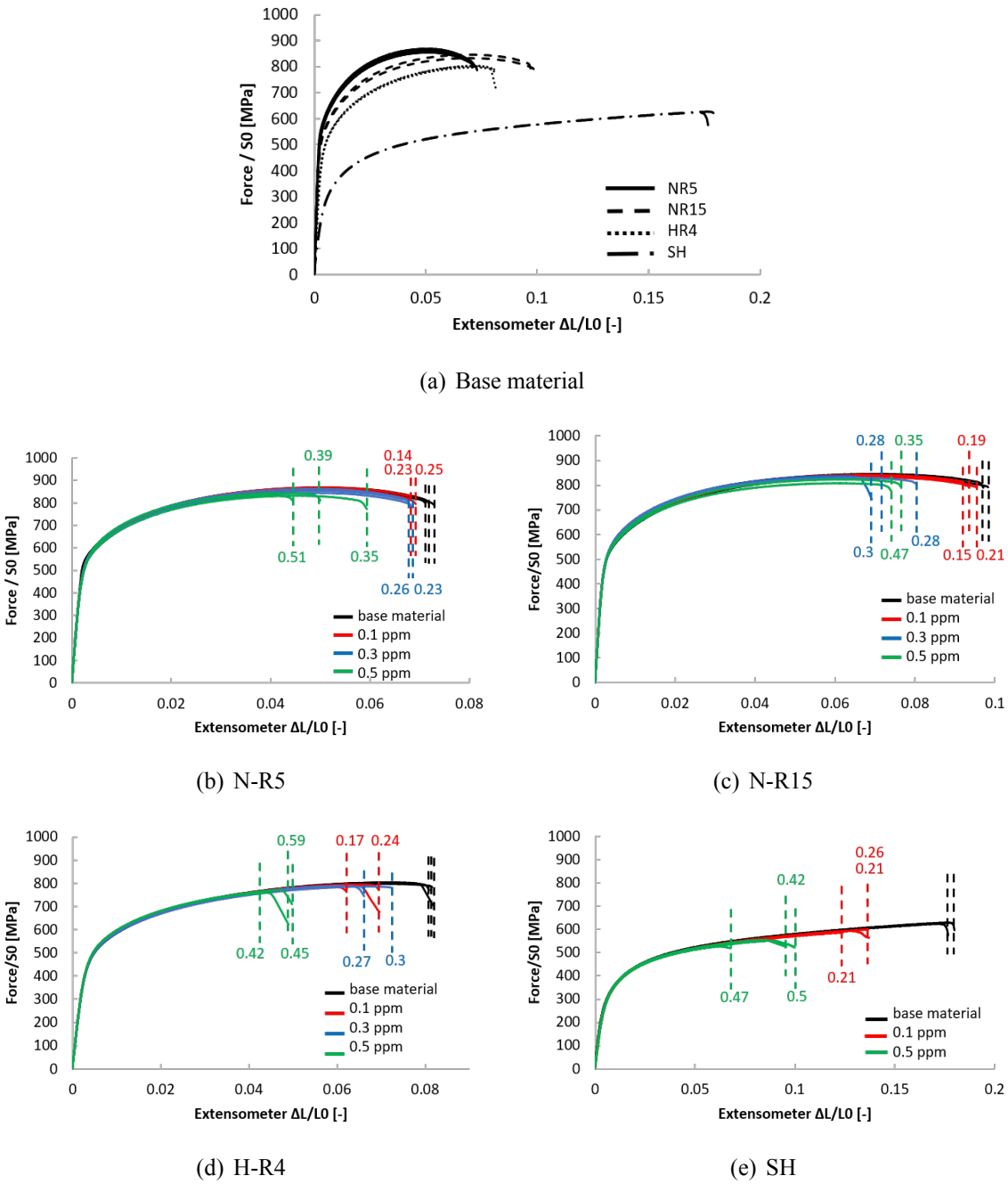

(a) Base material

(b) N-R5

(c) N-R15

(d) H-R4

(e) SH

Fig. 3: Evolution of the load divided by the initial minimum area as a function of the local elongation for rupture tests, for different hydrogen contents; the gauge length of the virtual extensometer is L_0 is around 15 mm for all the geometries. The color of the curves corresponds to the theoretical diffusible hydrogen content while the value given close to each curve corresponds to the measured one in ppm.

by:

$$\frac{(\Delta L/L_0)_{base} - (\Delta L/L_0)_i}{(\Delta L/L_0)_{base}} \tag{2}$$

with i corresponding to the different hydrogen contents, is calculated and shown in Table 3. This global indicator depends on the specimen geometry and on the hydrogen content. The relative decrease varies in-between $30\,\%$ and $60\,\%$ for hydrogen content of 0.5 ppm. However, it should be emphasized that rupture for SH geometry is sensitive to the edge quality, as shown further in this paper and therefore the apparent sharp increase of the indicator can not be attributed fully to a material effect. The tendency

for the smaller hydrogen contents (theoretical values) is less clear and should be confirmed with the measured values.

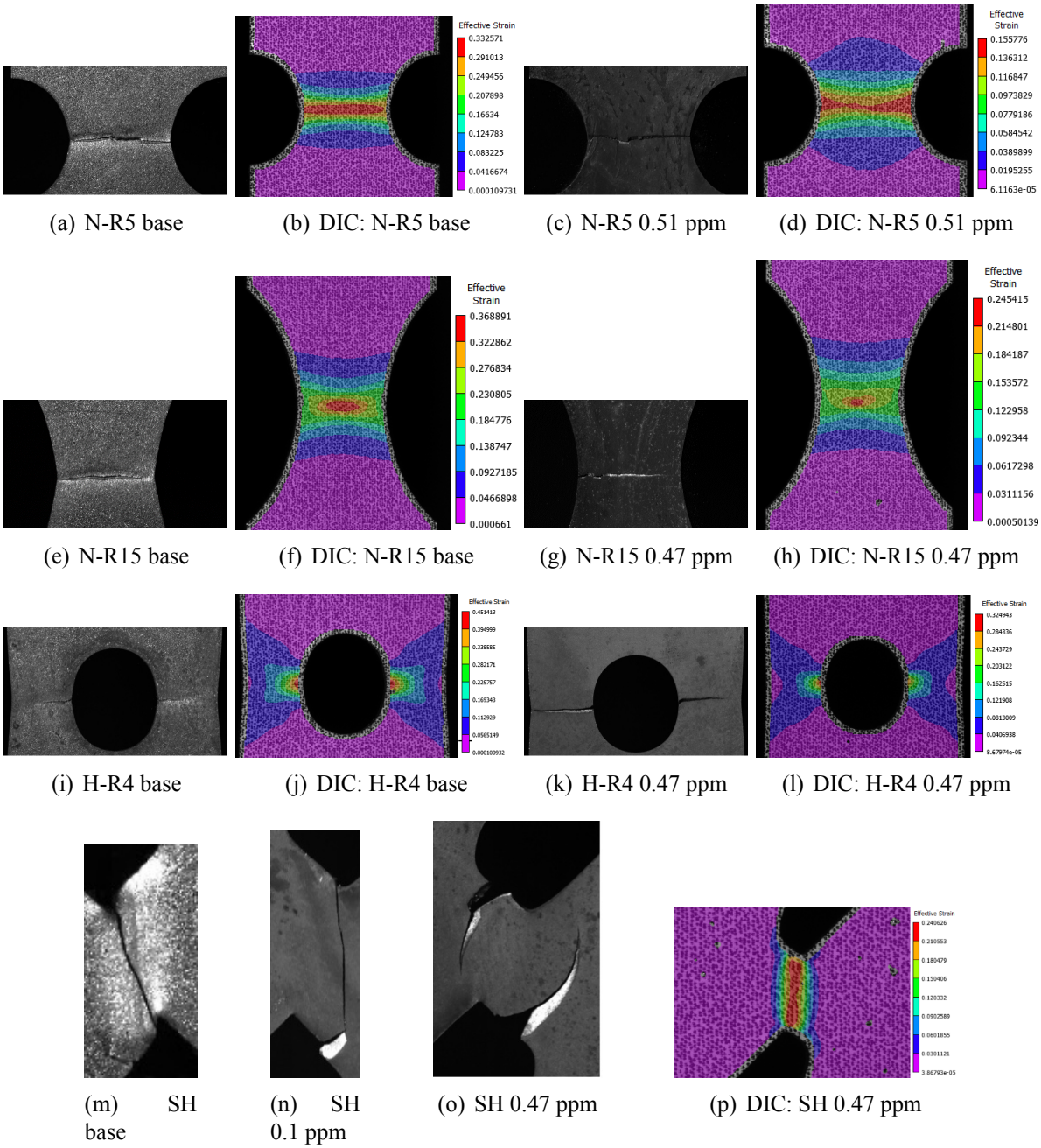

(a) N-R5 base (b) DIC: N-R5 base (c) N-R5 0.51 ppm (d) DIC: N-R5 0.51 ppm

(e) N-R15 base (f) DIC: N-R15 base (g) N-R15 0.47 ppm (h) DIC: N-R15 0.47 ppm

(i) H-R4 base (j) DIC: H-R4 base (k) H-R4 0.47 ppm (l) DIC: H-R4 0.47 ppm

(m) SH base (n) SH 0.1 ppm (o) SH 0.47 ppm (p) DIC: SH 0.47 ppm

Fig. 4: Crack location for the rupture tests, taken with the high-speed camera and isovalues of the effective strain just before rupture (or at the onset of the first crack for SH specimen).

Cracks occurred in the areas of maximum effective strain for N-R5, N-R15 and H-R4, whatever the hydrogen content (except for N-R15 and 0.5 ppm). Fig. 4 shows the images taken with the high-speed camera just before rupture, as well as the isovalues of the effective strain calculated with digital image correlation. It highlights the fact that the crack starts in the specimen center for notched specimen, except for a high hydrogen content where the crack starts from the edge, although the maximum effective strain is higher at the center of the specimen. This result is consistent with previous observations [4]. For H-R4, the crack always starts from the edge, whatever the hydrogen content. Moreover, only the side at which rupture occurred is used here. It should be emphasized that the effective strain measured by DIC is not at the edge but away fro mit by around 0.3 mm. In the case of the shear-type

Table 3: Evolution of the global indicator defined by Eq. 2 for the 4 geometries and the hydrogen contents. The average value is given, with also the minimum and maximum ones in brackets.

Hydrogen content [ppm]	N-R5	N-R15	H-R4	SH
0.15 ± 0.02	0.06	0.05	0.24	-
0.2 ± 0.02	-	0.04	-	0.27
0.25 ± 0.02	0.05	-	0.14	0.46 (0.24/0.62)
0.3 ± 0.02	-	0.25 (0.18/0.29)	0.15 (0.12/0.19)	-
0.35 ± 0.02	0.18	0.22	-	-
0.4 ± 0.02	0.31	-	0.44 (0.39/0.49)	
0.45 ± 0.02	-	-	0.39	-
0.5 - 0.6	0.39	0.24	0.40	0.44

specimen (SH), a different pattern is observed. Indeed, for the 3 base material specimens, a fracture line from the 2 opposite edges is observed, though a premature small crack appeared in the area where the 2 radius connect. For hydrogen-charged materials, this premature crack is the onset of the final rupture. This leads to a slow load decrease, corresponding to an apparent stable crack propagation but no longer in shear. Therefore, the maximum effective strain is taken at the onset of the premature crack occurence, representing a lower bound.

Influence of hydrogen on ductility. The evolution of the effective strain with the hydrogen content, for all the tests presented in this study, is shown in Fig. 5.

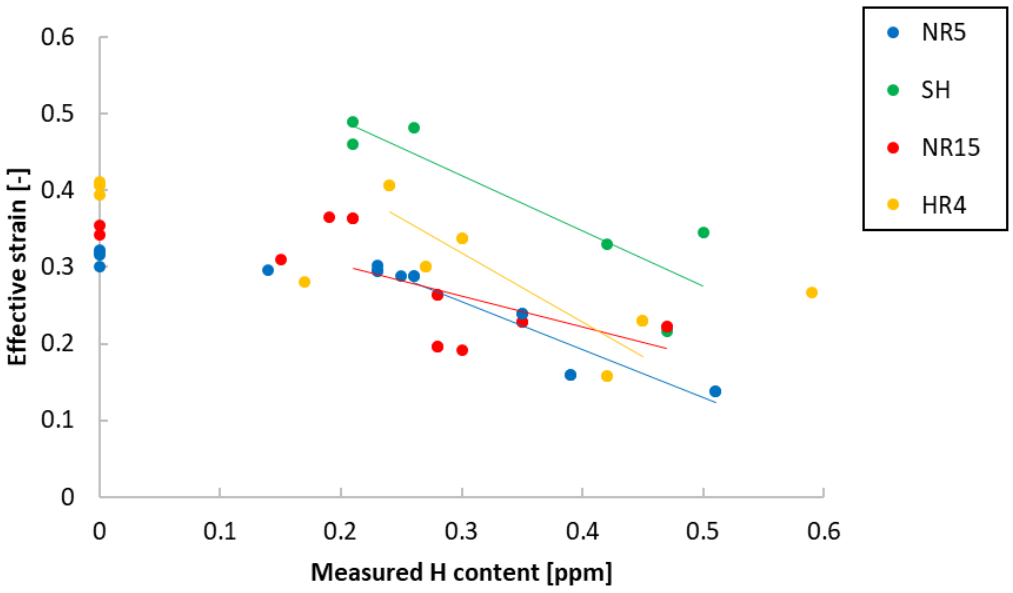

Fig. 5: Evolution of the maximum effective strain just before rupture for all the tests, except SH, for which the value is a lower bound as explained in the text. The solid line represents the linear regression done for each type of test, for hydrogen content in between 0.3 ppm and 0.5 ppm.

It can be seen that, as expected from previous studies, it decreases significantly whatever the mechanical state. A sensitive decrease is recorded for hydrogen contents between 0.25 ppm to 0.5 ppm. For the base materials, the decrease of the maximum effective strain with an increase of the stress triaxiality is observed. A linear regression of the evolution of the maximum effective strain with the measured hydrogen content was performed for each test, for hydrogen contents in-between 0.25 ppm

and 0.5 ppm. Indeed, for lower values, no significant variation is measured whatever the test and there is a lack of data for higher values. The slope is dependent on the sample geometry, having a higher absolute value for H-R4 than for N-R5. This result needs further investigation in relation to the hydrogen embrittlement mechanisms and the influence of the mechanical state. As rupture did not occur in the specimen center for SH, the regression slope for this test is not relevant.

Conclusions

The aim of this study is to investigate the influence of hydrogen content on the flow stress and the ductility for several mechanical states defined by different triaxiality ratios and Lode parameters using dedicated rupture tests. A dual phase steel DP780GI was provided as sheets of thickness 1 mm. Diffusible hydrogen content was imposed by cathodic charging for theoretical values ranging from 0.1 ppm to 0.5 ppm and then measured after the tests by thermal desorption analysis. The results are listed below:

- Although the experimental conditions were the same regarding the hydrogen charging, an apparent dispersion on hydrogen content is measured. Further analysis is under way to get a better understanding. However, the strength of the study is to provide quantified data on both hydrogen content and stress and strain data, not always available in literature.
- Fracture location and strain localisation are analysed to derive a representative quantity of the ductility limit of the material, measured on the specimen surface by Digital Image Correlation.
- The maximum effective strain dependence on diffusible hydrogen content seems dependent on the sample geometry, for values between 0.25 and 0.5. However, This result needs further investigation in relation to the hydrogen embrittlement mechanisms and the influence of the mechanical state.

Acknowledgements

The research leading to these results has received funding from the European Union Horizon Europe programme under grant agreement No 101157237 – H2FORM3G project [8]. The authors acknowledge ArcelorMittal for providing the materials, as partners of H2FORM3G project and A. Aouafi, T. Dieudonné and A. Kacem for fruitful discussions.

References

[1] T. Depover, D. Pérez Escobar, E. Wallaert, Z. Zermout and K. Verbeken: Int. J. Hydrogen Energy Vol. 39 (2014), 4647-4656

[2] S.K. Dwivedi and M. Vishwakarma: Int. J. Hydrogen Energy Vol. 44 (2018), 28007-28030

[3] A. Kumar and S.K. Paul: Forces in Mechanics Vol. 13 (2023), 100237

[4] T. Depover, A. Elmahdy, F. Vercruysse, P. Verleysen and K. Verbeken: EPJ Web of Conferences Vol. 183 (2018), 03015

[5] C. Zhao, W. Wu, J. Deng, M. Yu, Y. Peng, X. Wang and J. Gong: Eng. Failure Analysis Vol. 166 (2024), 108880

[6] M. B. Djukic, G. M. Bakic, V. S. Zeravcic, A. Sedmark and B. Rajicic: Eng. Fracture Mech. Vol. 216 (2019), 106528

[7] W. Zhao, W. Chen, Z. Zhao, S. Kuang, J. Liu and L. Sun: Mater. Res. Express Vol. 8 (2021), 126510

[8] H2FORM3G website https://eurecat.org/portfolio-items/h2form3g/

[9] B. Pan, Z. Jiang, F. Shen, B. Tekkaya and S. Munstermann: Steel Research Int. (2025), 2500266

[10] P. Prislupcak, T. Kvackaj J. Bidulska, S. Nemeth, M. Demcakova, R. Gburik and V. Kundracik: Acta Metall. Slovaca Vol 28 (2022), 212-218

[11] R.S. Varanasi, M. Koyama, Y. Shibayama, S. Chiba, S. Ajito, T. Hojo and E. Akiyama: Metall. Mater. trans. A 54 (2023), 2989-2997

[12] A. Kacem, H. Laurent and S. Thuillier: Eng. Fracture Mech. Vol. 248 (2021), 107686

[13] T. Omura: Steel Research Int. 52 (2012), 267-273

[14] T. Depover, S. Hertelé and K. Verbeken: Eng. Fracture Mech. Vol. 221 (2019), 106704